16th Australasian Fluid Mechanics Conference
Crowne Plaza, Gold Coast, Australia
2-7 December 2007

The Effect of a Uniform Cross-flow on the Circulation of Vortex Rings

E. R. Hassan, R. M. Kelso and P. V. Lanspeary

School of Mechanical Engineering
University of Adelaide, South Australia, 5005, AUSTRALIA

Abstract

This paper describes observations and measurements of the effects of a uniform cross flow on the vorticity field and circulation of a laminar vortex ring ejected from an elevated pipe. From particle-image velocimetry (PIV) in the plane defined by the axis of the vortex ring and the direction of the cross flow, we observe the growth and decay of the vortex-ring and its interaction with the shear layer which is produced by the cross flow over the surface of the elevated pipe. As the vortex ring is generated it passes through and disrupts this shear layer. Some rotational fluid from the shear layer is carried with the vortex ring as it moves away from the elevated pipe.

From the PIV data, we calculate a positive-core circulation on the upstream side of the vortex ring and a negative circulation on the other side. The growth rate of positive-core circulation is reduced by cancellation with the cross-flow shear-layer vorticity which is of opposite sign. The initial negative circulation is equal to the circulation of the cross-flow shear layer, but the cross flow and the cross-flow shear layer have *no* effect of the growth rate of the negative circulation.

Introduction

This study is motivated by the experimental observations that the penetration of a jet into a cross-flow can be increased by modulating the jet flow-rate. Both Johari *et al.* [8] and Eroglu & Breidenthal [4] demonstrate this phenomenon by using a solenoid valve to periodically stop and restart the flow of a jet in cross-flow. Both groups observe that pulsation of the jet flow at low frequencies produces a train of vortex-ring-like structures that convect further into the cross-flow than a continuous jet of the same ejection velocity.

Chang & Vakili [1] show that, in a train of sufficiently spaced vortex rings, each vortex ring acts independently of its neighbours. There is almost no interaction between vortices. This suggests that results from experiments with single or isolated vortex rings may also be valid for a sequence of vortex rings.

In this study we investigate the generation and subsequent development of a single vortex ring in a uniform cross-flow. From velocity measurements in the plane defined by the axis of the vortex ring and the cross-flow direction, we obtain the vorticity and the circulation of principal structures in the developing flow field.

Apparatus

Experiments are conducted in a closed-return water channel with a working section of 500 mm $\times$ 500 mm $\times$ 2000 mm. A vortex ring is generated by impulsively translating a piston within a clyinder for a short period. In this context "impulsively translating" means that the ideal piston velocity is a square-wave function of time. A stepper motor driving a lead screw advances the piston in a controlled and repeatable manner. Fluid from the cylinder flows through a hose into an elevated pipe which is shown schematically in figure 1. The elevated pipe has a diameter of D=25 mm and an exit plane which is 2.5D above the floor of the water channel. The axis of the elevated pipe is perpendicular to direction of the cross-flow, and the outside of the pipe is tapered at an angle of 7^o to a sharp edge at the tip.

PIV Method

Velocity components in the plane defined by the axis of vortex ring and the direction of the cross-flow are measured by two-component Particle Image Velocimetry (2C-PIV). The flow is seeded with 8 μm mean-diameter hollow glass spheres of a specific gravity 1.1. Illumination is provided by a dual-cavity Quantel Brilliant B Nd:YAG laser. The wavelength of the laser light is 532 nm and the duration of each laser pulse is approximately 5 ns. From the laser beam, an optics train generates a light sheet of thickness 1.5 mm. The PIV images are recorded by a Kodak Megaplus ES 1.0 CCD camera with an array of 1008 pixels $\times$ 1018 pixels and a Nikon 70-300 mm zoom lens. The image region is approximately 90 mm $\times$ 90 mm giving a spatial resolution of 11 pixels/mm. PIV image pairs are collected at a rate of 10 Hz with a time delay of 10 ms between the laser pulses illuminating the first and second images in each pair. A Stanford DG535 pulse-delay generator regulates the triggering of the laser pulses from each laser cavity. XCAP-Plus software collects and transfers images to computer hard disk as uncompressed 16-bit TIFF files. PIV velocity vectors are obtained by cross correlation of the image pairs. An interrogation-window size of 32 pixels $\times$ 32 pixels is used with 50% overlap. Correlation peaks are detected using a multi-pass double correlation, least squares Gaussian fit. Anomalous velocity vectors (outliers) are detected using a custom-built code which implements the universal median technique described by Westerweel and Scarano [11]. Detected outliers are replaced with a weighted average of valid surrounding vectors. For all results presented here, the number of outliers in any one velocity-vector field is less than 3% of the total number of vectors. An adaptive Gaussian window interpolator filters noise from the raw vector field.

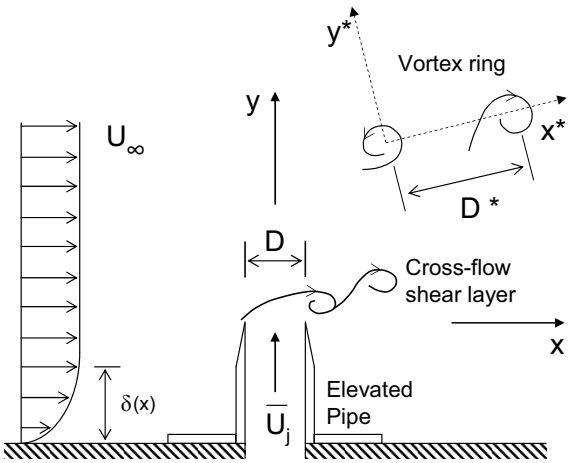

Figure 1: Flow and geometric parameters of the vortex ring in cross-flow.

U_∞ (mm/s)	$R = \overline{U}_j/U_\infty$	$Re_\infty = U_\infty D/\nu$	Number of Realisations
0	∞	0	47
6.0	6.2	150	56
11.0	3.4	270	58
21.8	1.7	550	47

Table 1: Cross-flow velocities, velocity ratios and cross-flow Reynolds number. Bulk jet velocity $\overline{U}_j \approx 37.2$ mm/s and $Re_\Gamma \approx 690$.

The estimated maximum error in the velocity measurements is 8%. This error is evaluated for the worst-case conditions where the velocity gradient is largest. Elsewhere the error is significantly smaller.

Procedure

The duration of piston motion is 1 second and the bulk-jet velocity over this time is $\overline{U}_j$=37.2 mm/s. The period of piston motion corresponds to a nondimensional time of $\widetilde{t} = t\overline{U}_j/D = 1.5$. The Reynolds number of the vortex ring is most appropriately defined in terms of the circulation of the vortex ring, $Re_\Gamma = \Gamma/\nu$ The vortex slug model described in Shariff and Leonard [10] provides a convenient estimate of the circulation, Γ_{slug} so that

$$Re_\Gamma = \frac{\Gamma_{slug}}{\nu} \approx \frac{\frac{1}{2}\overline{U}_j^2 \tau}{\nu}. \quad (1)$$

For the current data $Re_\Gamma \approx 690$. The length of the extruded fluid slug is $L \approx 1.5D$.

Four flow conditions are investigated, each at a different ratio of bulk-jet velocity, $\overline{U}_j$, to the cross-flow velocity, U_∞. The velocity ratio, $R = \overline{U}_j/U_\infty$, is varied by changing the cross-flow velocity. Table 1 describes the experimental conditions; i.e. the cross-flow velocities, velocity ratios and cross-flow Reynolds numbers (Re_∞). Note that, without a cross flow, $R \to \infty$ and $Re_\infty = 0$. To ensure statistical reliability, data collection is repeated approximately 50 times at each velocity ratio; Table 1 gives the exact number.

A custom-built electronic controller synchronises the start of vortex generation with the next available laser pulse and enables the camera trigger. This ensures that the n-th PIV image pair in any one realisation is synchronised with the n-th image pair in all other realisations.

Tests conducted at $Re_\infty \approx 450$ show that, slightly upstream of the pipe, the Blasius boundary layer on the floor of the water channel has a thickness of $\delta(x) \approx 0.8D$. The boundary layer thickness is much smaller than the height of the elevated pipe. Measurements made with a cross-flow only (in the absence of a vortex ring) show the presence of a vortex-shedding shear layer at the top of the elevated pipe. This "cross-flow shear layer" is shown schematically in figure 1 and by dye visualisation in figure 2.

Data Processing

The out-of-plane vorticity field, ω_z, of each time step of each realisation is estimated from the in-plane velocity components. The hybrid compact-Richardson extrapolation (CR4) vorticity-estimation scheme of Etebari & Vlachos [5] is a noise-optimised, fourth-order scheme which simultaneously reduces both the random error and the bias error. This vorticity estimation scheme is applied to all the data. Applying the error propagation analysis of Fouras & Soria [6] gives maximum random and bias errors which are 7.3% and 5.9% respectively of the peak vorticity value. The maximum total error in vorticity is

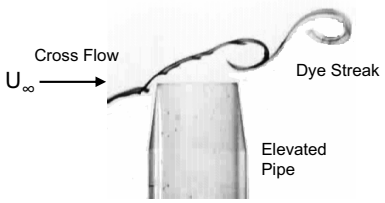

Figure 2: Flow visualisation of the cross-flow shear layer in the absence of a vortex ring

therefore 9.4% of the peak vorticity value. Vorticity is presented in the nondimensional form, $\widetilde{\omega} = \omega_z D/\overline{U}_j$.

Circulation, Γ, of each vortex core is estimated by numerically integrating velocity components around the boundary of a region in which vorticity exceeds a threshold value. For this investigation, the threshold level is $\widetilde{\omega}$=0.4, which corresponds to approximately 4% of the peak vorticity. Details of the method and the associated error analysis are given in Hassan *et al.* [7]. The estimated total error in circulation is 5.1%. Circulation is presented in the nondimensional form, $\widetilde{\Gamma} = \Gamma/(\overline{U}_j D)$.

Vorticity and circulation are calculated for each realisation and at each of 50 time steps.

Evolution of the vorticity field, $\widetilde{\omega}$ (Figure 3)

In the absence of a cross flow, the vortex ring forms as the piston pushes fluid from the elevated pipe, and the vortex ring moves away along the axis of symmetry of the pipe. Figure 3 shows the nondimensional vorticity field of the vortex ring at nondimensional time $\widetilde{t}$=5.2 after the start of piston motion for velocity ratios $R \to \infty$ and R=3.4. Two cross-sections of the vortex ring are visible in figure 3(a). The cross-section on the left has positive vorticity and, for convenience, is referred to as the positive core. The cross-section on the right has negative vorticity and is referred to as the negative core. Also for convenience, we define the center of each vortex core as the location of the local maximum of absolute vorticity. The cores initially grow in time but remain equal in size; they remain symmetrically disposed about the axis of the pipe. Remnants of the stopping vortex, which is generated by cessation of piston motion, are visible at the pipe exit.

With the addition of a uniform cross flow, we still observe the development of the two vortex cores but many of the details are different. The self-induced motion of the vortex ring is augmented by convection in the direction of the cross flow as shown by comparing figure 3(b) with figure 3(a). The vortex ring tilts as it moves into the cross-flow; we observe that the line between vortex cores tilts at an angle of up to 25 degrees from the cross-flow direction. The direction of tilt angle is given by the vector cross product $\mathbf{U}_\infty \times \overline{\mathbf{U}}_\mathbf{j}$. Chang & Vakili [1] report similar tilting in trains of vortex rings in which the vortex rings are well separated.

With the addition of a uniform cross flow, even before vortex generation, there is a region of negative vorticity near the top of the elevated pipe. This is the "cross-flow shear layer" (figure 2). As the vortex ring is generated it passes through and disrupts the shear layer. The shear layer begins to re-form when the vortex core is sufficiently far from the elevated pipe. As we observe the progress of events in the vorticity field, the negative core seems to combine with the negative vorticity in the shear layer and so seems to become larger. Some negative vorticity from the cross-flow shear layer is carried with the negative core as it moves away from the elevated pipe. Observation of the evolving vorticity field shows that as the negative core convects

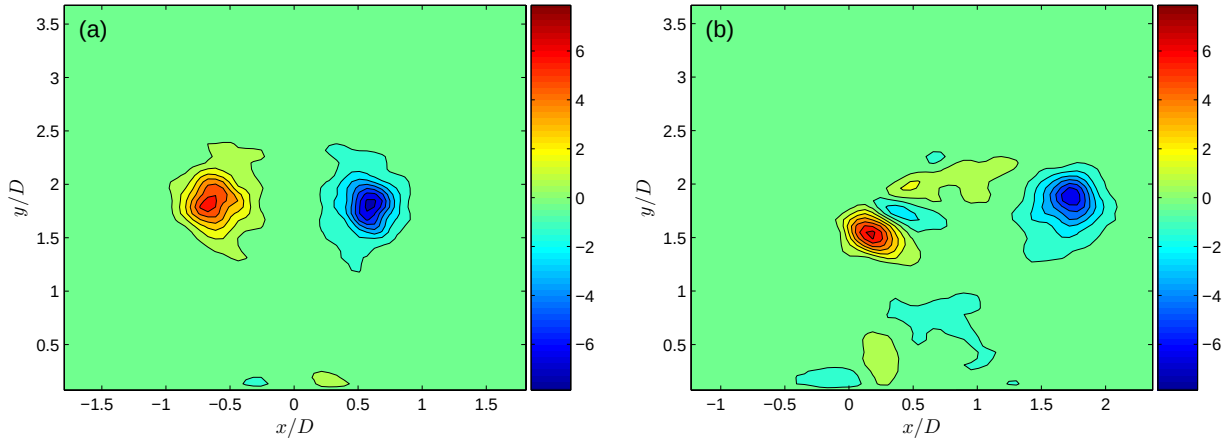

Figure 3: Vorticity field, $\widetilde{\omega}$, of the vortex ring, at $\widetilde{t}$=5.2, (a) in the absence of a cross-flow ($R \to \infty$) and (b) in a R=3.4 cross flow.

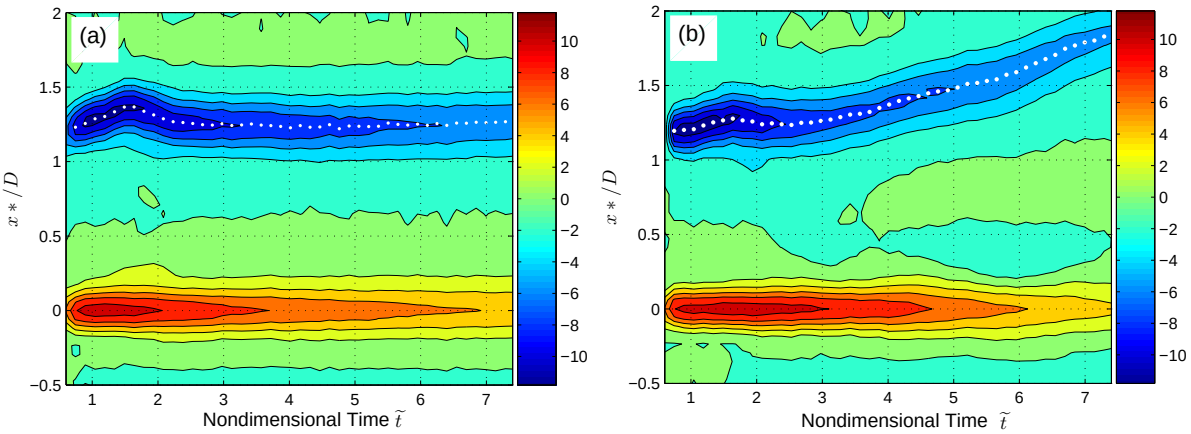

Figure 4: Ensemble-averaged vorticity distribution along the line connecting the vortex cores (a) in the absence a cross-flow ($R \to \infty$) and (b) in a R=3.4 cross-flow. Maximum vorticity is at $x^*/D = 0$. The distance between vortex centers is shown as a sequence of white dots.

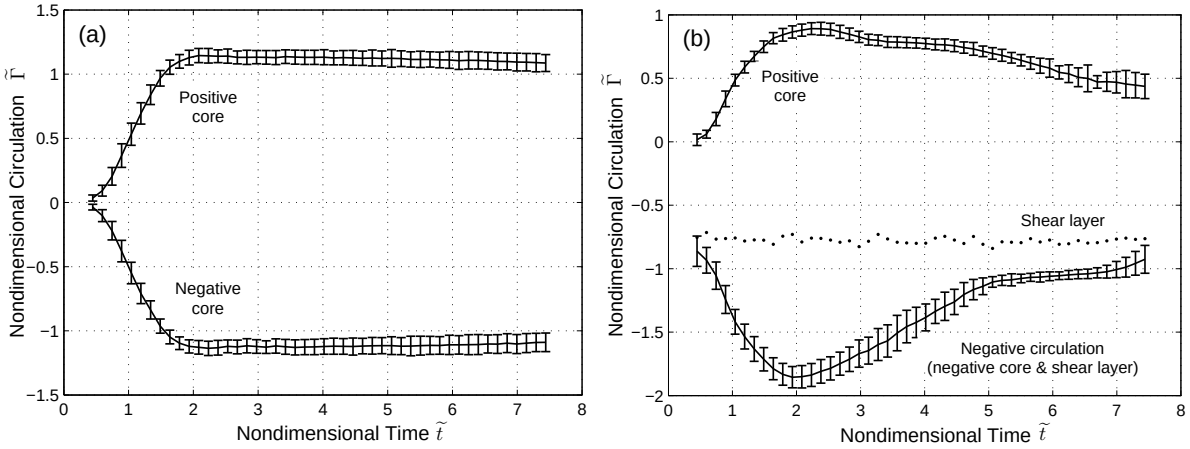

Figure 5: Growth and decay of ensemble-averaged circulation (a) in the absence of a cross-flow ($R \to \infty$) and (b) in a R=3.4 cross-flow. The errorbars show 95% confidence limits on the ensemble-averaged circulation. The symbols • in (b) show the circulation of the cross-flow shear layer in the absence of a vortex-ring.

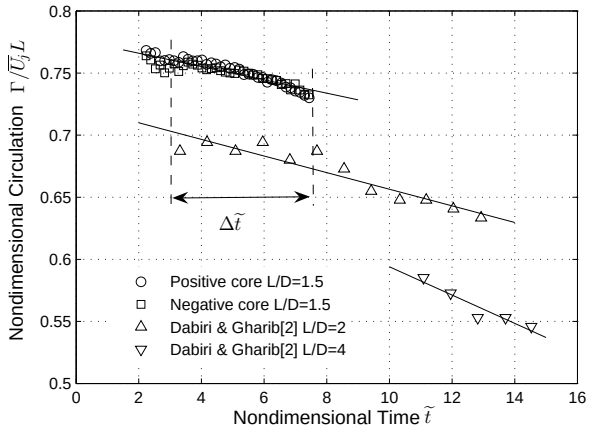

Figure 6: Decay of the absolute circulation of the vortex ring cores in the absence of a cross-flow, $R \to \infty$.

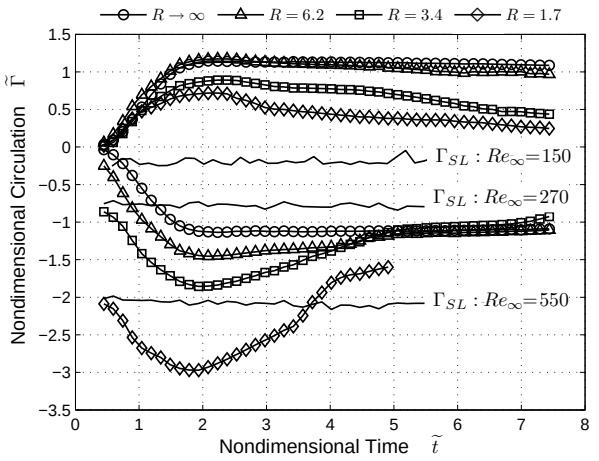

Figure 7: Growth and decay of ensemble-averaged circulation for all four velocity ratios. The solid lines show circulation (Γ_{SL}) of the cross-flow shear layer in the absence of a vortex-ring.

into the cross-flow, it sporadically sheds structures containing negative vorticity. Meanwhile the size of the positive core remains approximately constant. Another feature of this flow, as shown in figure 3(b), is the existence of structures of opposite sign vorticity between the two principal cores. Initially, these structures are not apparent; they appear as the vortex ring convects into the cross-flow. At the interface between the positive core and the adjacent negative vorticity structure there is a high vorticity gradient which suggests high local rates of diffusion.

Distortion of the vortex ring (Figure 4)

To measure the distance between the vortex cores and to plot the distribution of vorticity between them, we map the vorticity-field data onto a new coordinate system (x^*, y^*) which moves with the vortex cores. The origin (x^*, y^*)=$(0,0)$ is at the centre of the positive core and the x^* axis joins the centres of the vortex cores as shown in figure 1. The mapping is performed at every time step and for every realisation. At each time step the vorticity distribution along the x^* axis is ensemble averaged over all the realisations and is plotted in figure 4 as a function of time. The distance between vortex centres, which is a characteristic diameter D^* of the vortex ring, is shown in figure 4 as sequences of white dots.

In the absence of a cross-flow (figure 4(a)), the vortex-ring diameter, D^* increases steadily up to a maximum of about 1.4D at $\tilde{t}$=1.5 when the piston stops. The diameter then decreases and levels out at about 1.25D. Similar observations were made in the experiments of Didden [3] and the numerical simulations of Nitsche and Krasny [9]. After $\tilde{t}$=2 the vorticity distribution between the cores remains almost anti-symmetric about the mid-point between vortex cores. Deviation from anti-symmetry is probably due to variation in D^* from one realisation to another. Inspection of individual realisations shows that they are indeed anti-symmetric.

With the addition of a cross-flow (figure 4(b)), the vortex ring increases in diameter to 1.3D until $\tilde{t}$=1.5. Thereafter the diameter contracts slightly and then increases steadily to about 1.8D at $\tilde{t}\approx$7.2. This stretching of the vortex ring is observed whenever there is a cross-flow. After $\tilde{t}\approx$3.5 regions of negative vorticity can be seen near the positive core at $x^*/D \approx 0.4$. This vorticity is from the negative-vorticity structure which‘ develops between the principle cores and can be seen in figure 3.

Development of circulation (Figures 5 & 6)

Figure 5 shows the growth and decay of ensemble-averaged circulation of the vortex ring. The error bars show 95% confidence limits on the ensemble average.

In the absence of a cross-flow (figure 5(a)), the magnitudes of circulation in both vortex cores increases linearly with time, $\tilde{\Gamma} \sim \tilde{t}$. They reach a maximum a short time after the piston stops at $\tilde{t}$=1.5, and then they decay.

Dabiri and Gharib [2] measure the circulation of vortex rings with stroke ratios of $L/D = 2$ and $L/D = 4$. In order to compare the Dabiri and Gharib data with our no-cross-flow data, circulation in figure 6 is nondimensionalised using the slug length L rather than diameter D. Figure 6 shows that, in the time interval Δt containing both $L/D = 1.5$ and $L/D = 2$ data, the average difference in circulation is 8%. Decay rates are obtained by fitting straight lines to the data in figure 6. Dabiri and Gharib [2] clearly obtain a somewhat smaller decay rate for $L/D = 2$ than for $L/D = 4$. Our $L/D = 1.5$ data have an even smaller decay rate and so are consistent with the hypothesis that decay rate of circulation increases with slug ratio L/D.

The development of circulation is significantly changed with the addition of a cross-flow (figure 5(b)). The • symbols in the figure show the circulation of the cross-flow shear layer in the absence of a vortex ring. As we observe the evolving vorticity field, the region of negative vorticity in the cross-flow shear layer combines with the region of negative vorticity identified as the “negative (vortex) core”. Circulation is calculated by integrating the velocity around the boundary of a region in which vorticity exceeds a threshold, and so the negative circulation in figure 5(b) contains contributions from both the negative vortex core and the cross-flow shear layer. On the other hand, the calculation of positive circulation includes only the positive vortex core. Clearly in figure 5(b) the initial value of the negative circulation is the same as the circulation of the cross-flow shear layer.

When the piston is in motion, both negative circulation and positive-core circulation increase steadily until a short time after the piston stops at $\tilde{t} = 1.5$. The positive-core circulation and the negative circulation decay thereafter, at different rates and at a higher rates than without a cross flow. Negative circulation decays faster than the positive-core circulation. Negative circulation includes a contribution from the cross-flow shear layer which rolls up almost periodically after it is shed from the top

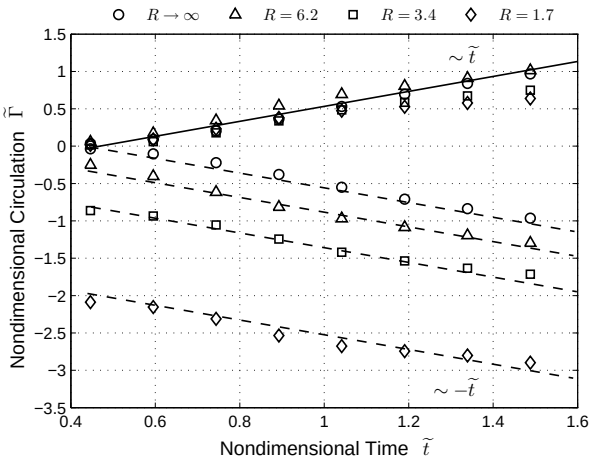

Figure 8: Growth of nondimensional circulation during vortex generation. The slope of the solid line is +1; the slope of each dashed line is -1.

of the elevated pipe. Vortex rings are generated without synchronising with any particular phase of shear-layer roll up, and so the negative circulation has wider confidence intervals than the positive-core circulation.

Rate of change of circulation

Figure 7 shows the growth and decay of the ensemble-averaged circulation at all four velocity ratios. Solid lines in the figure show circulation (Γ_{SL}) of the cross-flow shear layer in the absence of a vortex-ring. The figure shows that the rate of change of circulation

$$\dot{\widetilde{\Gamma}} = \frac{d\widetilde{\Gamma}}{d\widetilde{t}} = \frac{1}{U_j^2}\frac{d\Gamma}{dt}, \qquad (2)$$

is significantly effected by the presence of a cross-flow. Figure 8 shows the growth of nondimensional circulation during the vortex generation period $\widetilde{t} \lesssim 1.5$.

For the positive cores with cross flow, we observe that $\dot{\widetilde{\Gamma}}$ is initially the same as without cross-flow but gradually decreases. This decrease occurs as the positive vortex core passes through the region of negative vorticity in the cross-flow shear layer. The presence of the cross flow leads to a lower maximum circulation in the positive core. From figure 8, the presence of the cross-flow appears to have little effect on the rate of change of negative circulation.

Figure 7 shows that, for $2 \lesssim \widetilde{t} \lesssim 5$, cross flow has the effect of increasing the rate of decay of the negative circulation. This is consistent with the observation that as the negative core passes through the cross-flow shear layer, it first "picks up" rotational fluid of the shear layer and then "sheds" it. Cross flow also induces a larger rate of decay of circulation in the positive cores but for a different reason. In the positive cores, the higher rate of decay is due to destructive diffusion between the positive core and a region of negative vorticity which appears between the principal vortex cores (as shown in figure 3(b)).

Conclusions

We obtain velocity (PIV) measurements of a vortex ring ejected from an elevated pipe into a uniform cross flow. From these measurements, we observe the growth and decay of the vortex-ring and its interaction with the shear layer which is produced by the cross flow over the surface of the elevated pipe. As the vortex ring is generated it passes through and disrupts this shear layer. Some rotational fluid from the shear layer is carried with the vortex ring as it moves away from the elevated pipe.

From the PIV data, we calculate a positive-core circulation on the upstream side of the vortex ring and a negative circulation on the other side.

1. The growth rate of positive-core circulation is reduced by cancellation with shear-layer vorticity of opposite sign.
2. The initial negative circulation is equal to the circulation of the cross-flow shear layer, but the cross flow and the cross-flow shear layer have *no* effect of the growth rate of the negative circulation.
3. Over the nondimensional time interval $2 \lesssim \widetilde{t} \lesssim 5$, the effect of cross flow is to increase the rate of decay of both positive and negative circulations. The decay rates vary with the cross-flow speed.

Acknowledgments

The first author has received scholarships from the University of Adelaide. Apparatus used for this research has been built and purchased with funds from the ARC.

References

[1] Chang, Y. and Vakili, A., Dynamics of vortex rings in cross-flow, *Physics of Fluids*, **7**, 1995, 1583–1597.

[2] Dabiri, J. and Gharib, M., Fluid entrainment by an isolated vortex ring, *Journal of Fluid Mechanics*, **511**, 2004, 311–331.

[3] Didden, N., On the formation of vortex rings: rolling-up and production of circulation, *Journal of Applied Mathematics and Physics (ZAMP)*, **30**, 1979, 101–116.

[4] Eroglu, A. and Breidenthal, R., Exponetially accelerating jet in cross flow, *AIAA Journal*, **36**, 1998, 1002–1008.

[5] Etebari, A. and Vlachos, P., Improvements on the accuracy of dervative estimation from DPIV velocity measurments., *Experiments in Fluids*, **39**, 2005, 1040–1050.

[6] Fouras, A. and Soria, J., Accuracy of out-of-plane vorticity measurements derived from in-plane velocity field data, *Experiments in Fluids*, **25**, 1998, 409–430.

[7] Hassan, E., Lau, T. and Kelso, R., Accuracy of circulation estimation schemes applied to discretised velocity field data, in *Proceedings of the Sixteenth Australasian Fluid Mechanics Conference, Gold Coast, Australia*, The University of Queensland, 2007.

[8] Johari, H., Pacheco-Tougas, M. and Hermanson, J., Penetration and mixing of fully modulated turbulent jets in cross flow, *AIAA Journal*, **37**, 1999, 842–850.

[9] Nitsche, M. and Krasny, R., A numerical study of vortex ring formation at edge of a circular tube, *Journal of Fluid Mechanics*, **276**, 1994, 139–161.

[10] Shariff, K. and Leonard, A., Vortex rings, *Annual Review of Fluid Mechanics*, **24**, 1992, 235–279.

[11] Westerweel, J. and Scarano, F., Universal outlier detection for PIV data, *Experiments in Fluids*, **39**, 2005, 1096–1100.